



# The Two Zones of Floor Failure and its Control via a ‘Dual Key Layer’ Approach

Wei Miao<sup>1,2</sup> · Yanchun Xu<sup>1</sup> · Dongyu Guo<sup>1</sup> · Chaorui Xing<sup>1</sup> · Bosong Zhang<sup>1</sup> · Lei Li<sup>3</sup> · Jun Li<sup>1</sup>

Received: 11 July 2023 / Accepted: 10 February 2024 / Published online: 18 March 2024  
© The Author(s) under exclusive licence to International Mine Water Association 2024

## Abstract

In the Jiaozuo mining area of the North China coal field, there are multiple water-rich aquifers close to the coal seam. To prevent water inrush accidents, the subfloor strata needs to be reinforced by grouting before mining. According to how the mechanics and hydrogeological properties of the key floor rock strata changed after grouting, the coal seam floor was divided into two zones: a ‘water conductive fracture zone’ and a ‘mechanically strong damaged zone’. A composite model of a key structurally stable water-control floor layer and a key infiltration-water damage-control floor layer was established after grouting of the uppermost (L8) subfloor aquifer. Microseismic (MS) technology was used to analyze the characteristics of the two zones and the water control capability of the two key layers in faulted and non-faulted regions of the experimental working face, which revealed that the grouted L8 limestone served as a key mechanical barrier layer. The change in the elastic modulus of the rock mass before and after grouting was measured by the borehole ultrasonic method, which showed that the elastic modulus of the rock mass increased by 40–852% after grouting. Based on FLAC3D numerical simulation and field measurements, grouting reduced the failure depth of the floor by 51%. Seven factors that influence the floor water control ‘dual key layers’ were proposed, which were quantified using the analytic hierarchy process (AHP) method. We found that fault activation and water-filled faults were the main factors affecting the water control capability of the dual key layer. The results of the research will contribute to the early warning, prevention, and evaluation of floor water inrushes in mines with similar hydrogeological conditions.

**Keywords** Floor failure · Floor water control dual key layer · Microseismic · Analytic hierarchy process · Floor water inrush

## Introduction

In the mining areas of central and eastern China, the threat of floor-confined water is becoming increasingly dire as coal mining depth has increased (Li et al. 2022; Liu et al. 2022). Some mines are seriously threatened by floor-confined water, such as in the Jiaozuo and Hanxing mining areas in the North China coal field, where mining is threatened by multiple water eruptions from a limestone aquifer that is less than 20 m thick and a deeper limestone aquifer that is

more than 400 m thick. Subfloor grouting is usually used to reinforce and reform the floor strata before mining (Hu et al. 2019; Quiel et al. 2019; Zhai and Bai 2023). This decreases the water-richness of the closer aquifer, and fills the cracks, reducing the threat of a floor water inrush.

Many scholars have carried out research on the use of floor grouting reinforcement in water-abundant mining areas. Zhai et al. (2022) proposed a secondary grouting-reinforcement method to ensure that sufficient grout would be injected into the aquifer. Zuo et al. (2022) studied the temporal and spatial characteristics of rock fractures in the floor of deep mines using rock fracture microseismic (MS) data; the results showed that the energy inoculation level of fracture expansion around the aquifer decreases after grouting. Mu et al. (2023) proposed an evaluation method for a grouted floor based on mining-induced MS data and studied the fracturing zone and stress distribution for different grout radii. Andrews and Keim (2021) assessed cases

✉ Wei Miao  
wilson09@126.com

<sup>1</sup> School of Energy and Mining, China University of Mining and Technology, Beijing Campus, Beijing 100083, China

<sup>2</sup> Jiaozuo Coal Industry Group, Jiaozuo 454000, Henan, China

<sup>3</sup> Jiulishan Coal Mine, Jiaozuo 454002, Henan, China

of underground mines beneath streams in recent decades, analyzed methods of grouting, and made recommendations to avoid inrushes.

The failure of the surrounding rock is often closely related to water inrush. Michasa and Vallianatos (2020) used concepts of statistical physics to study the spatiotemporal and diffusion properties of micro-seismicity and investigated the possible involvement of fluids in the triggering mechanism. Ma et al. (2021) investigated the response characteristics of key strata during the periodic weighting process in the Dongjiahe coal mine by MS monitoring and identified the fracture types of key strata. Xu et al. (2022) developed a method for determining hydraulic parameters by integrating the induced MS data collected during hydraulic stimulation with tracer test data from the subsequent trial production period, which was verified and applied to the Habanero enhanced geothermal system in Australia. Huot et al. (2022) created a curated dataset of nearly 7000 manually selected MS events and an equal number of background noise examples and optimized a deep learning model's network architecture together with its training hyperparameters by Bayesian optimization, which increased the accuracy of the analysis.

Floor water inrush still occurs occasionally in the working face during mining despite grouting. Based on the mechanical formula derivation, MS monitoring, and transient electromagnetic (TEM) detection, this study focused on how the mechanical and hydrogeological properties of the key rock strata was changed by grouting, establishing a 'dual key layer' in the strata below the mine floor, and the factors that might influence potential water control failures in this 'dual key layer'.

## Engineering Overview

The Jiulishan coal mine is located in the Jiaozuo mining area of Henan Province, China. According to the hydrogeological characteristics of the coal field, the main aquifers below the coal seam are, from top to bottom, the L8, L2, and O2 limestone aquifers. Where the limestone is more than 8 m thick and the occurrence is stable, the aquifers are strong or extremely strong. The aquiclude between each limestone is mainly composed of thin weak water-rich hard rock and argillaceous soft rock. Where the mudstone and sandy mudstone is thicker than 10 m and stable, an effective aquiclude is formed. Floor grouting is conducted before mining based on the water inrush coefficient, but water inrush still occurs in a few of the working faces during mining.

The 15,091 working face is located in the east wing of the Jiulishan Mine (Fig. 1). The average thickness of the 2–1 coal seam is 5.5 m. The full-thickness fully mechanized

top-caving coal mining method is being used; the average mining height is 5.0 m, the average roadway length is 425 m, the working face length is 110 m, and the maximum buried depth is 460 m. There are two faults in the working face, namely the F15-14 fault (with a vertical fault throw of 2.8–3.0 m) and F15-15 fault (with a vertical fault throw of 0.5–4.8 m). The L8 limestone aquifer is 8.5 m thick, 23 m below the 2-1 coal seam, and has a water pressure of 1.9 MPa. According to the hydrogeological data, the unit water inflow of the L8 limestone is 0.00019–5.4 L/s·m. The L2 limestone aquifer is about 12 m thick, 75 m below the 2–1 coal seam, the water pressure is 3.8 MPa, and the unit water inflow is 0.785–2.430 L/s·m. The O2 limestone aquifer is 107 m below the coal seam, the water pressure is 5.7 MPa, and the unit water inflow is 0.395–5.249 L/s·m (Fig. 2). To avoid a floor water inrush, the L8 limestone aquifer and faults are grouted before mining; the range of grouting reinforcement is 66.5 m from the 2–1 coal (35 m from the bottom of the L8 limestone). Measured by the direct current method, the depth of the floor failure zone is 15 m.

## Characteristics of the Two Zones of the Working Face Floor

### Definition of the Two Zones

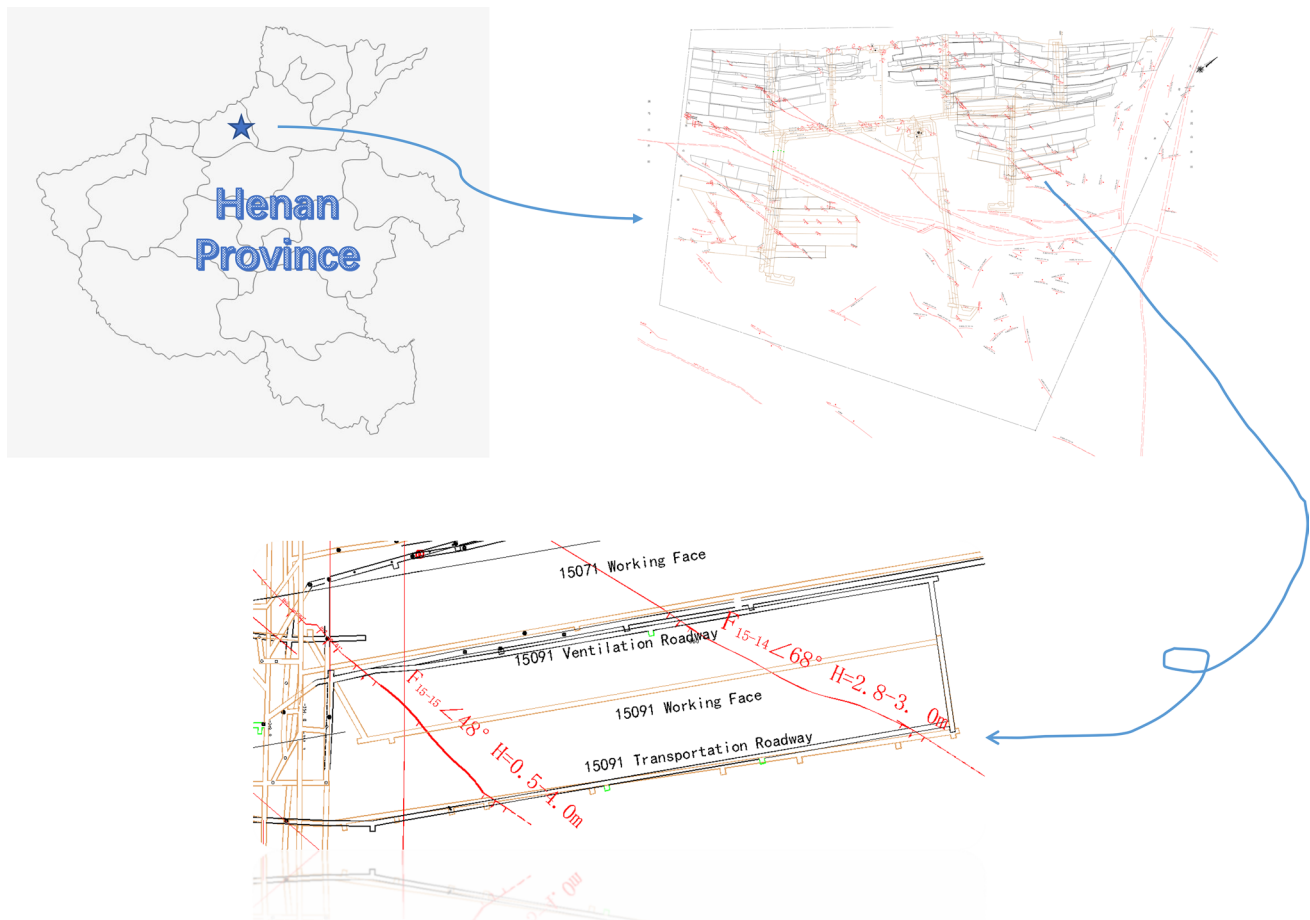
#### Water Conductive Fractured Zone

The 'water conductive fractured zone' refers to the significant plastic failure of the floor rock layer after mining. Even though the failure zone does not extend directly to the confined aquifer below, the water pressure is sufficient to break through the residual barrier layer. The confined water only needs to overcome the resistance of the channel and the remaining aquiclude to cause a floor water inrush.

For example, the L8 limestone is 23 m below the 2–1 coal seam in the 15,091 working face, and the water pressure is 1.9 MPa, and the depth of the floor failure zone is 15 m. Without floor grouting reinforcement, the remaining 8 m of aquiclude cannot prevent the L8 confined water from rushing into the working face during mining, producing an inrush. Therefore, the range of the water-conductive fracture zone is from the 2–1 coal seam to the L8 limestone (23 m).

#### Mechanical Strength Damaged Zone

The 'mechanical strength damaged zone' refers to the disconnected fractured zone in the aquiclude between the upper aquifer and deep aquifer, which is formed under the influence of the pre-mining primary rock stress and post-mining failure stress. The fractures in the zone are mainly primary



**Fig. 1** Mine and researching working face location

fractures, and the natural stress is the main factor that forms the early deformation of the intact rock mass. Mining can cause the vertical stress on parts of the surrounding rock to exceed the failure strength of the rock mass; when this occurs, the cracks in the local rock mass extends and penetrates along the impact direction, destroying the integrity of the original and grouted rock strata. Because the force is mainly from the mining activity and the deep confined water, the water-conducting fractures are generally vertical and in a small area.



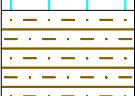

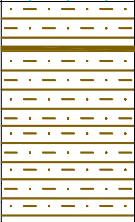
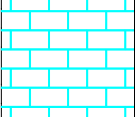

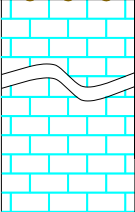
## MS Characteristics of the Two Zones of the Floor

### Construction of the MS System

MS events represent damage by mining stress (Xiao et al. 2023a, b). In general, the number of MS events reflects the activity level of the surrounding rock, and the macroscopic damage is caused by the accumulation of microcracks. Using multiple sets of high-sensitivity detectors installed in the working face roadways, MS monitoring captures the tiny

vibrations generated by rock fracturing during the formation of a water inburst channel, so that the MS events can be located (Miao et al. 2022).

The 15,091 working face MS monitoring system mainly includes MS sensors, an underground digital signal acquisition master station, a digital signal processing system, and a real-time monitoring platform. The response frequency range of the MS sensors was 0.1–600 Hz, with a sensitivity of 100 V/s/m. 11 sensors were arranged on the working face, of which 6 were installed in the ventilation roadway (1#–6#) and five were installed in the transportation roadway (7#–11#). A 20 mm diameter anchor rod is required to install a sensor, and more than 0.5 m of the anchor rod needs to be embedded in the roof (or floor). The sensor is fixed on the anchor rod to ensure that the geophone installation direction is vertical. The sensor spacing is 100 m. In Fig. 3, the floor sensors are marked as green spots and the roof sensors are marked as red spots. To test the positioning accuracy of the MS monitoring system, blasting was carried out in the working face after construction of the MS system, and the hypocenter was identified.

Thickness (m)	Stratum	Lithology
4.9–5.8		2-1Coal
8.9–10.2		Mudstone
0.90–2.27		L9 Limestone
6.3–8.7		L8 Limestone
35.0–55.0		Sandy mudstone
9.8–15.1		L2 Limestone
10.5–22.1		Aluminaceous mudstone
>400m		O2 Limestone

**Fig. 2** Comprehensive histogram of coal seam floor

Mining of the 15,091 working face started on November 21, 2020, and the MS monitoring system has been in operation since January 14, 2021. The monitoring area is 39.7 m<sup>2</sup> and a total of 1130 MS events have been detected. The MS events energy is 15.5–5690.1 J, with an average of 310.7 J, and a magnitude of  $-0.05 \sim 1.31$  on the Richter scale. The MS events range from 212 m above the working face to 129.9 m below.

#### Number and Energy Distribution Characteristics of Floor MS Events

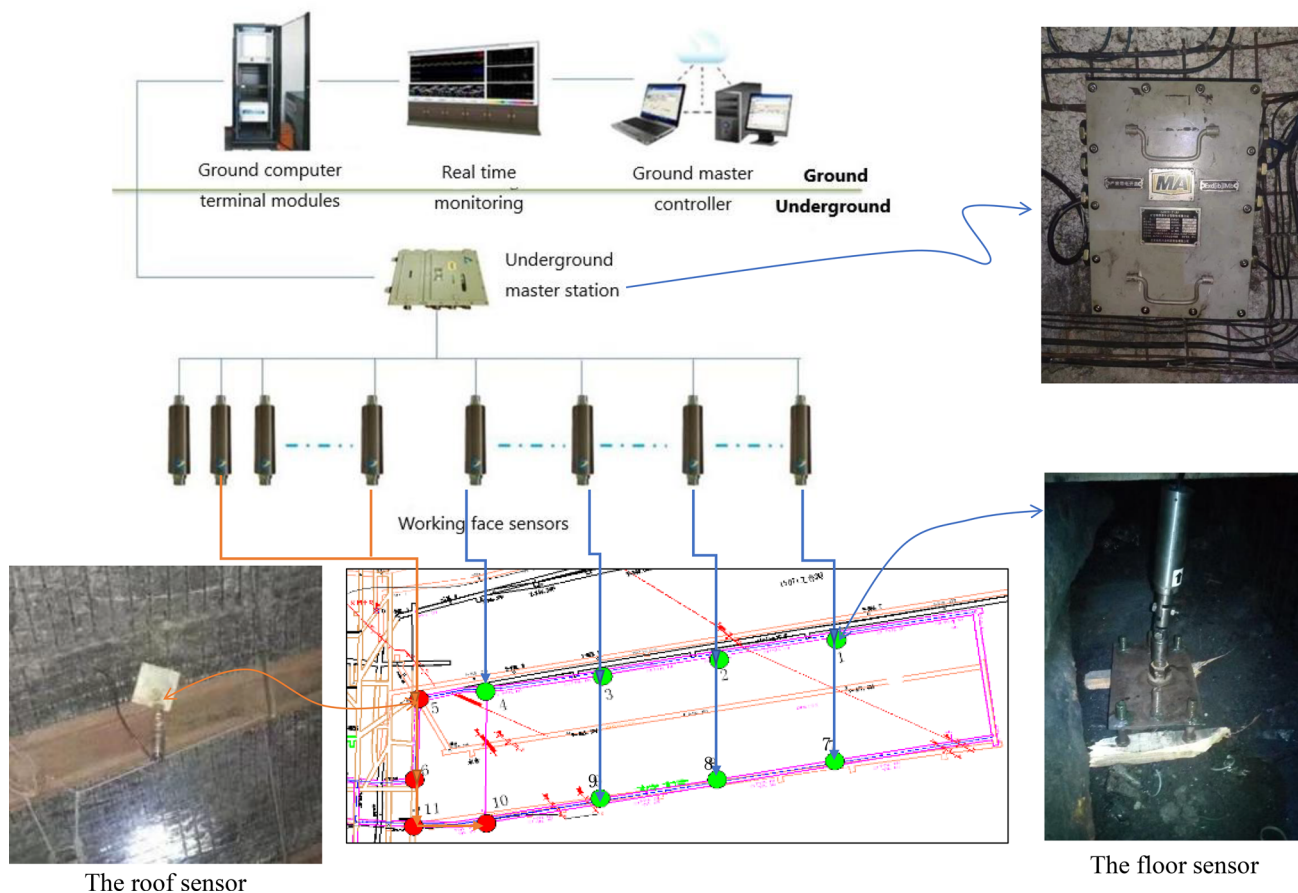
As shown in Fig. 1, there is no fault in the central region of the 15,091 working face, which is defined as a normal mining region. From March 1 to April 30, the working face advanced 126 m in this region and 64 floor MS events were detected. Of the 64 events, 52 events occurred in the floor failure zone, accounting for 81% of the total (Fig. 4). There were four MS events (6%) between the floor failure zone and the L8 limestone bottom interface and eight (13%) below the L8 limestone. The peak value of MS events was consistent with the range of the floor failure zone. Compared with the number of MS events in the floor failure zone, the number of MS events below that zone was reduced by 92.3%, which indicates that the main factor causing floor failure in the normal mining region was the mining stress of the working face.

The MS energy ranged from 15.6 J to 1213.9 J, including 48 (about 75%) MS events with energy levels less than 500 J. 15 (about 23%) of the MS events had energy levels of 500 J to less than 1000 J, and only one (about 2%) MS event exceeded 1000 J. There was an inverse relationship between the MS energy and the number of MS events in the 45 m range below the working face. The MS energy increased gradually with depth, while the corresponding MS events number decreased sharply. The MS energy in the range of 45–75 m below the working face decreased markedly with greater depth, while the MS energy events number were stable at 2–3, indicating that the energy source was still from mining stress and that the stress gradually decreases with increased depth. As shown in Fig. 3, a small energy MS event appears at the end of the energy curve, located on the F15-15 fault plane, indicating that the deep fault plane was activated to some extent.

#### Distribution Characteristics of MS Morphology in the ‘Two Zones’ of the Floor

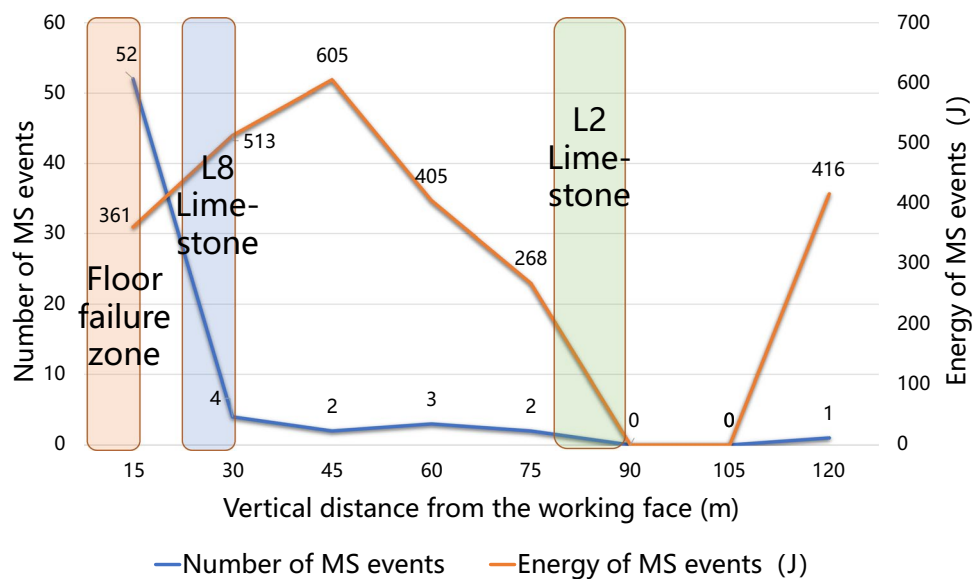
The MS event distribution profile diagram of the 15,091 working face is shown in Fig. 5. The MS events morphology presents the distribution characteristics of the two zones with obvious differences: the upper MS events were concentrated in the floor failure zone, showing a ‘inverted saddle-type’ stress distribution feature (black dashed line in Fig. 5a), which is basically consistent with the mining floor failure pattern, indicating that the mining activity was the main factor changing the floor stress in this zone.

There were only five low-energy MS events in the mechanical strength damaged zone, which were concentrated between the L8 limestone and L2 limestone (orange



**Fig. 3** Layout of microseismic system

**Fig. 4** Relationship diagram of MS events energy, number and vertical distance



dashed line in Fig. 5a); the distribution characteristics were separate or horizontal. Due to its proximity to the L2 limestone aquifer, the MS energy source is not only from the

working face, but also caused by uplifting of the confined L2 limestone water.



Cloud maps of MS event density generated by ARCGIS software comprise Fig. 5b, c. It can be seen from Fig. 5b that the floor MS event density cloud was basically located within the floor failure zone. The high-density area was mainly located in the ventilation roadway near the goaf, and the density gradually decreases with depth, indicating that the failure pattern of the floor was mainly affected by the working face mining stress. The five MS events above the L2 limestone were relatively discrete. The MS energy density cloud (Fig. 5c) shows that the energy source was from the mining activity.

Due to the special hydrogeological conditions in the Jiaozuo mining area, the L8 limestone aquifer is relatively close to the coal seam. After the floor was damaged by mining stress, the residual floor 8 m aquiclude of the 15,091 working face could not resist the upward disturbance of the confined water and the mining fractures easily connected to the lifting fractures of L8 limestone confined water. The range of the water conductive fracture zone was deeper than the floor failure zone.

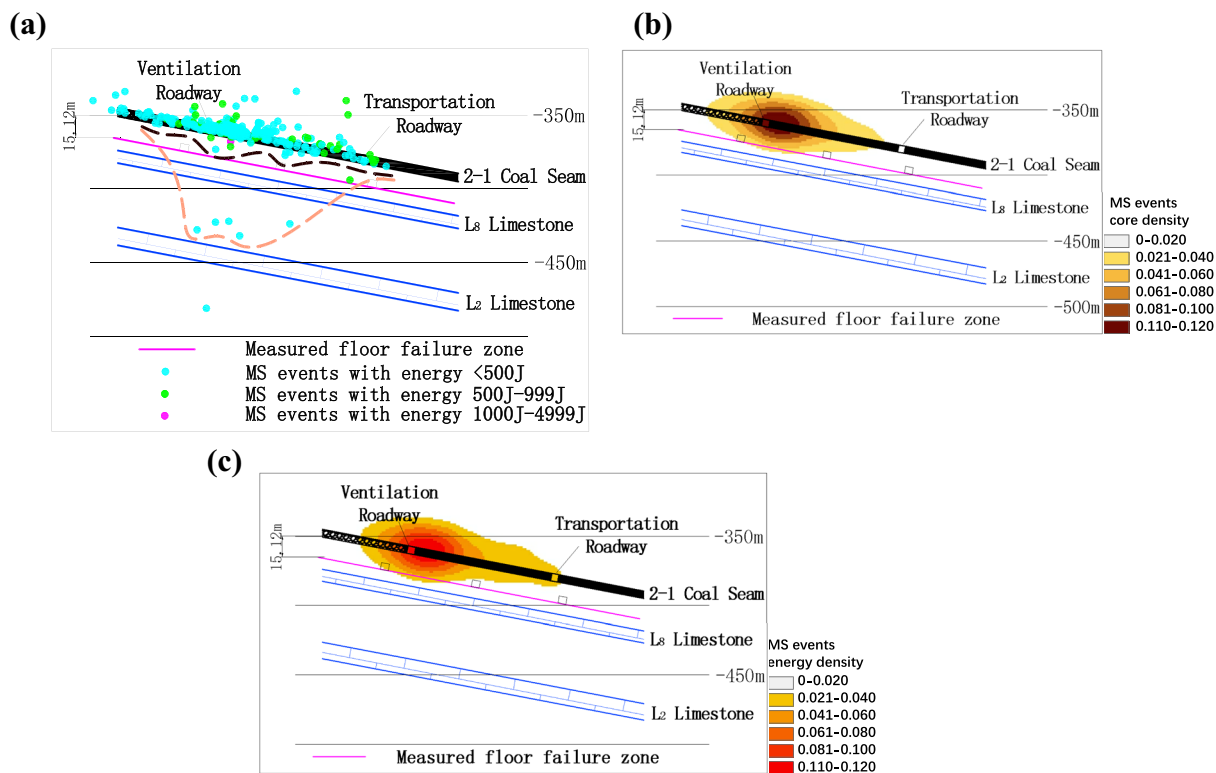
In normal mining regions, the mechanical strength damage of the deep rock layer would be more influenced by the primary rock fissure and the lifting stress of the L2 limestone

aquifer. In this zone, discontinuous rock mechanical damage occurs only in a small range, the distribution characteristic of MS events was distinct or horizontal, and there was no connection with the upper water conductive fracture zone.

## The 'Dual Key Layer' Composite Water Control Mechanism of Floor Grouting Reinforcement

### The 'Dual Key Layer' Composite Water Control Model

To prevent a floor water inrush from the L8 limestone aquifer, floor grouting reinforcement was conducted before mining (as shown in Fig. 6), transforming the aquifer into a key stable water control layer. In addition, a certain thickness of strata beneath the L8 limestone was grouted, along with the underlying argillaceous rock mass, forming a key layer combination of structural stability. The upper structural-stability layer mainly acts as a mechanically stable beam structure, preventing failure of the working face and blocking the mining stress. The infiltration damage control layer (including the grouted strata beneath the L8 limestone) largely seals the



**Fig. 5** 15,091 working face floor MS events profile. **a** Scatter plot of MS events. **b** MS events core density cloud map. **c** MS events energy density cloud map

deep confined water fractures by increasing the mechanical characteristics of the rock mass. Therefore, the composite ‘dual key layer’ is both a mechanical supplement and a barrier, preventing a water inrush from the deep aquifer.

However, floor water inrush events still occurred in some working faces that had been grouted, which indicates that there are factors that can lead to the failure of the approach. Therefore, research was conducted to promote the prevention and control of future floor water inrush events.

### The Key Structurally Stable Floor Water Control Layer

According to the key layer theory, the stable key layer of the floor structure should be a thick rock layer (group) with high mechanical strength and poor water-richness, which critically resists floor deformation and mining-induced failure. The high strength strata between the coal seams and the Ordovician limestone aquifer in the North China coalfield are basically thin (less than 20 m) limestone layers, which are porous aquifers and cannot act as a key layer of water resistance. After grouting, the internal cracks and pores of the thin limestone layers are solidified and sealed by the slurry, so the thin limestone layers are transformed into poor aquifers or aquicludes. At the same time, their mechanical strength is reinforced by grouting, which enhances their floor-bearing capacity and reduces the deformation amount and damage. The grouted thin limestone layers thus become a key structurally stable water-control layer.

### The Key Floor-Damage Infiltration-Water Control Layer

The key floor-damaging infiltration-water control layer should be a thick rock layer (group) with good natural water-resistance and high resistance to the upward infiltration of deep confined water. As shown in Fig. 6, the aquifers are separated by soft rock aquicludes such as mudstone and sandy mudstone that swell with water and disintegrate, which can seal the water-filled fractures. The water control function mainly has two aspects: if the upper portion of the key structurally stable layer is broken by mining stress and the lower argillaceous aquiclude is thick (such as the argillaceous layer

between the L8 limestone and L2 limestone in the Jiaozuo mining area), the argillaceous soft layer will inhibit fracture extension. However, as the confined water rises, the argillaceous soft layer expands and disintegrates, which inhibits the cracks from connection.

### Division of the Two Zones Under the Condition of ‘Dual Key Layer’

After the L8 limestone is modified into a key structurally stable water-control layer by grouting reinforcement, floor rock failure is mainly caused by stope stress tensile shear failure caused by mining; the range of the water-conductive fracture zone is consistent with that of the floor failure zone.

The rock mass of the key floor damage infiltration water-control layer is influenced by both the indirect effects of the mining stress and the lifting stress of the L2 limestone aquifer. The mechanical strength damaged zone is composed of the part of the key structurally stable water-control layer, which is not in the vertical range of the water-conductive fracture zone, and the ‘key structurally stable floor-water control layer’.

### Influence of Grouting Reinforcement on Rock Mass Strength

#### Test Principle

Acoustic measurement of the rock mass is used to study the propagation velocity, deduce the related physical and mechanical state, obtain the elastic model, and provide a reference for evaluating the engineering quality of a rock mass. Due to the existence of cracks and structural planes, a rock mass cannot be regarded as an ideal uniform medium. From an engineering point of view, a rock mass can be regarded as a continuous isotropic linear elastic material when the ultrasonic wave is smaller than the spatial size of the measured original rock mass. The relationship between wave velocity and elastic modulus of a rock mass is as follows (Xu et al. 2017):

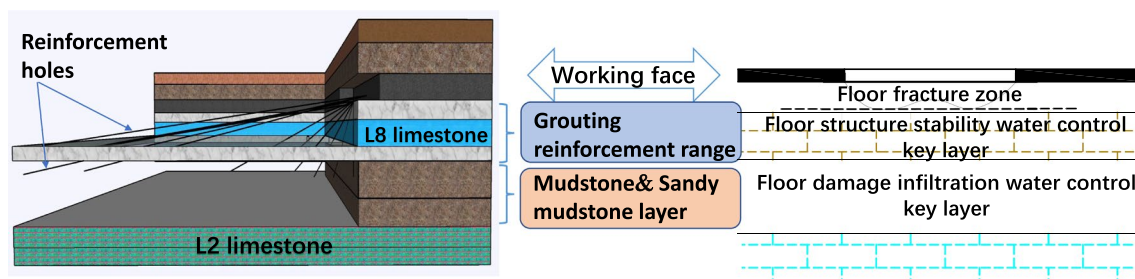


Fig. 6 Schematic diagram of dual key layer water control model

$$E_d = \frac{\rho(1 + \mu_d)(1 - 2\mu_d)}{1 - \mu_d} V_p^2 \quad (1)$$

$$\Delta E = E_d - E'_d \quad (2)$$

$$\lambda = \frac{E'_d - E_d}{E_d} \times 100\% \quad (3)$$

where:  $\rho$  is the rock mass density,  $\text{g/cm}^3$ ;  $E_d$  and  $E'_d$  are the dynamic elastic modulus of rock mass before and after grouting, respectively, GPa;  $\Delta E$  is the change of dynamic elastic modulus of rock mass before and after grouting, GPa;  $\mu_d$  is the dynamic Poisson ratio of the rock mass;  $V_p$  is the velocity of longitudinal wave in the rock mass; and  $\lambda$  is the reinforcement degree of the dynamic model of grout-reinforced rock mass.

### Test Method

The ZBL-U520 ultrasonoscope was used, which includes a transmitting transducer T and two receiving transducers R1 and R2 (Fig. 7a), where the distance L from T to R1 is the source distance and the distance between R1 and R2 is  $\Delta L$ . The search unit is placed in the drilling hole and the transducer T is stimulated by the ultrasonoscope to radiate sound waves. In the rock mass, the refraction angle of the sound wave is equal to  $90^\circ$ ; that is, the sound wave glides along the hole wall and then refracts back into the hole to be received by the receiving transducers, R1 and R2, respectively (Fig. 7b). The wave velocity inside the rock mass is calculated from the time difference,  $\Delta t$ , of sound wave propagation in the rock mass, providing the elastic mechanic parameters of rock mass. The dynamic elastic modulus,  $E_d$ , of the rock mass is measured by the ultrasonic method. The

static elastic modulus  $E_j$  of the rock mass can be obtained by conversion:  $E_j = 0.25E_d1.3$ .

### Measurement of Rock Mass Strength Change

In the 15,091 working face of the Jiulishan Mine, the elastic modulus of the grouted floor rock mass was measured by the borehole ultrasonic method. Meanwhile, the elastic modulus of the grouted and ungrouted floor rock mass was similarly measured in the 11,030 working face of Zhaogu coal mine which in the same mining area. The floor strata of the two working faces is basically the same, and the measuring area avoids the influence of working face mining and fault structure. Due to the metal casing at the vertical depth of 12 m from the exploration hole opening, the field measurement was carried out after the ultrasonic probe completely exited the casing and entered the rock layer vertically. Data was collected every 2 m, stopping at a position 4.5 m into the L8 limestone aquifer.

The results are shown in Table 1. It can be seen that the elastic modulus of different floor rock was enhanced by grouting, with the mudstone having the largest increase, (640–852%), followed by sandy mudstone with an increase of 241–641%, sandstone with 221–247%, L9 limestone with 176%, and L8 limestone with an increase of 40–159%. The argillaceous rocks are generally soft and cracks are more likely to occur under the influence of high-pressure grouting. After solidification of the grout-filled cracks, the elastic modulus of argillaceous rock mass increased greatly.

After detecting the elastic modulus of each rock formation, the weighted average compressive strength of the whole rock formation was obtained by means of the average modulus method:

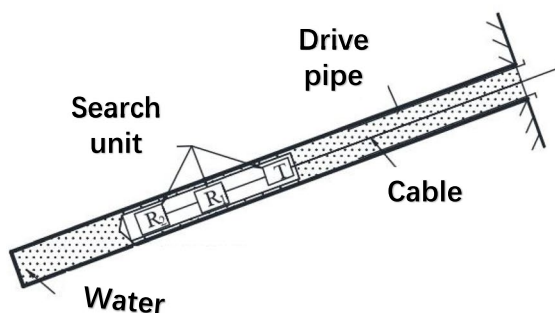


Fig. 7 ZBL-U520 ultrasonic detection equipment



$$\overline{R_c} = \frac{h_1 R_{c1} + h_2 R_{c2} + \cdots + h_i R_{ci} + \cdots + h_n R_{cn}}{h_1 + h_2 + \cdots + h_i + \cdots + h_n} = \frac{\sum_1^n h_i R_{ci}}{\sum_1^n h_i} \quad (4)$$

where:  $\overline{R_c}$  is the weighted average compressive strength of floor rock, MPa;  $h_i$  is the thickness of the no.  $i$  rock formation, m; and  $R_c$  is the compressive strength of the no.  $i$  stratum, MPa. The rock elastic modulus value of the casing section cannot be measured, so the elastic modulus of the same lithology was brought into the calculation. The relationship between uniaxial compressive strength and elastic modulus of sedimentary rocks is shown in Table 2 (He et al. 2011).

The converted compressive strength values of different floor strata were incorporated into formula (4). The results are shown in Table 3. Then, the calculated results of Table 5 were incorporated into the fracture mechanic formula of the floor failure zone depth:

$$h1 = \frac{1.57\gamma^2 h^2 L}{4\overline{R_c}^2} \quad (5)$$

where:  $\gamma$  is the average bulk density of the floor aquiclude,  $\text{N/m}^3$ , which is  $2.4 \times 10^4 \text{N/m}^3$ ;  $h$  is the mining depth (470 m);  $\overline{R_c}$  is the weighted average compressive strength of floor rock, which is brought into the calculation results in Table 3;  $L$  is the length of the working face (110 m). According to the calculated results: without grouting reinforcement, the floor failure depth was 30.6 m, which would cause the floor failure zone to directly connect to the L8 limestone aquifer, resulting in a water inrush.

After grouting reinforcement, the floor failure depth was calculated to be 11.7 m, and the floor failure depth was measured to be 15 m by the direct current method—a difference of 4.3 m. Note that most of the parameters used in the calculation were the average of the entire range of the mine or working face, and that the field measurement was mainly conducted in one appropriate location of the working face. The larger value of the two results was selected. Therefore, the failure depth of the grouting reinforced floor was about 51% less than the failure depth without grouting.

## Numerical Simulation Result

The FLAC3D software can realize the establishment of a 3D mining model, the distribution of geometric and mechanical parameters of the strata, the calculation of rock deformation and stress evolution, and a simulation analysis of mining. A 3D digital model was established using the actual rock thickness of the 15,091 working face and the rock lithology of the floor after grouting. The height, width, and thickness of the numerical model were 800, 410, and 313 m, respectively, containing a total of 311,480 units and 326,592 nodes. The thickness of each rock layer in the model was simulated based on the actual stratum thickness of the working face. In the initial stage, we ran the model to the equilibrium state, simulated the original mechanical state of the coal and rock, and excavated 20 m each time.

Figure 8 shows the simulated layout of the plastic zone at different advanced positions during mining of the 15,091 working face. With excavation of the coal seam, the original stress of the surrounding rock of the working face was broken, and the stress was redistributed, transferred, and transmitted. When the stress of the surrounding rock exceeded its critical strength, plastic failure occurred. A plastic zone was formed in the rock surrounding the excavation, resulting in stress concentrating around the coal seam. Due to stress release in the goaf, the stress was concentrated on both sides of the coal wall, and the plastic zone in the goaf gradually increased in scope. The failure form of the bottom plate was saddle-like and the maximum plastic failure depth was about 17 m. The numerical simulation of floor failure depth was

**Table 2** Relationship equation of uniaxial compressive strength and elastic modulus of sedimentary rock

Lithology	Relationship equation
Sandstone	$E = 0.0887R1.0851 \text{ C}$
Mudstone	$E = 0.0924R1.1339 \text{ C}$
Sandy mudstone	$E = 0.0186R1.7426 \text{ C}$
Limestone	$E = 0.0913R1.2053 \text{ C}$

**Table 1** Results of ultrasonic measurement of floor strata (elastic modulus unit: GPa)

Floor depth	Average value of elastic modulus			11,030 working face elastic modulus increment/(increase proportion) $E_z$	Working face elastic modulus increment/(increase proportion) $E_z$	Lithology
	11,030 working face before grouting $E_1$	11,030 working face after grouting $E_2$	15,091 working face after grouting $E_3$			
12–17.5 m	1.7	5.9	5.3	4.2 (247%)	3.6 (221%)	Sandstone
17.5–18.5 m	3.8	10.5	10.5	6.7 (176%)	6.7 (176%)	L9 limestone
18.5–23 m	1.7	5.8	12.6	4.1 (241%)	10.9 (641%)	Sandy mudstone
23–28.5 m	0.5	3.7	4.8	3.2 (640%)	4.3 (852%)	Mudstone
28.5–33.5 m	3.4	8.8	4.8	5.4 (159%)	1.4 (40%)	L8 limestone

**Table 3** Compressive strength of floor composite rock strata of 15,091 working face floor

Lithology	Thickness (m)	Elasticity modulus without grouting reinforcement (GPa)	Elasticity modulus after grouting reinforcement (GPa)	Converted compressive strength without grouting reinforcement (MPa)	Converted compressive strength after grouting reinforcement (MPa)	Compressive strength of floor composite rock strata without grouting reinforcement (MPa)	Compressive strength of floor composite rock strata after grouting reinforcement (MPa)
Mudstone	2.2	0.5	4.8	4.4	32.3	13.4	36.2
Sandy mudstone	3.8	1.7	12.6	13.3	42.1		
Sandstone	5.5	1.7	5.3	13.3	43.3		
L9 limestone	1.5	3.8	10.5	22.1	51.2		
Sandy mudstone	4.5	1.7	12.6	13.3	42.1		
Mudstone	5.5	0.5	4.8	4.4	32.3		
L8 limestone	8.5	3.4	4.8	20.1	26.6		

basically consistent with the analysis of floor failure depth measured by direct current method and MS monitoring.

## Influence Factors of ‘Dual Key Layer’ in the Grouting Reinforced Working Face

### Factors Influencing the Key Structurally Stable Water-Control Layer

By grouting reinforcement, the slurry fills the rock fractures, increasing the rock mechanical strength, and making the L8 limestone a key structurally stable water-control layer that blocks the downward transmission of mining stress and the lifting stress of the L2 limestone aquifer. It is mainly affected by the following four factors.

- (1) Space relationship between the floor failure zone and the key layer

Mining-induced failure is the main factor affecting the structural stability of the key layer. According to the spatial relationship, it can be divided into two cases: when the key layer is in the range of the floor failure zone or when it is deeper than the range of floor failure zone, that is, when the distance between the key layer and the working face ( $M$ )  $\leq$  the floor failure depth ( $h_1$ ), or when  $M > h_1$ .

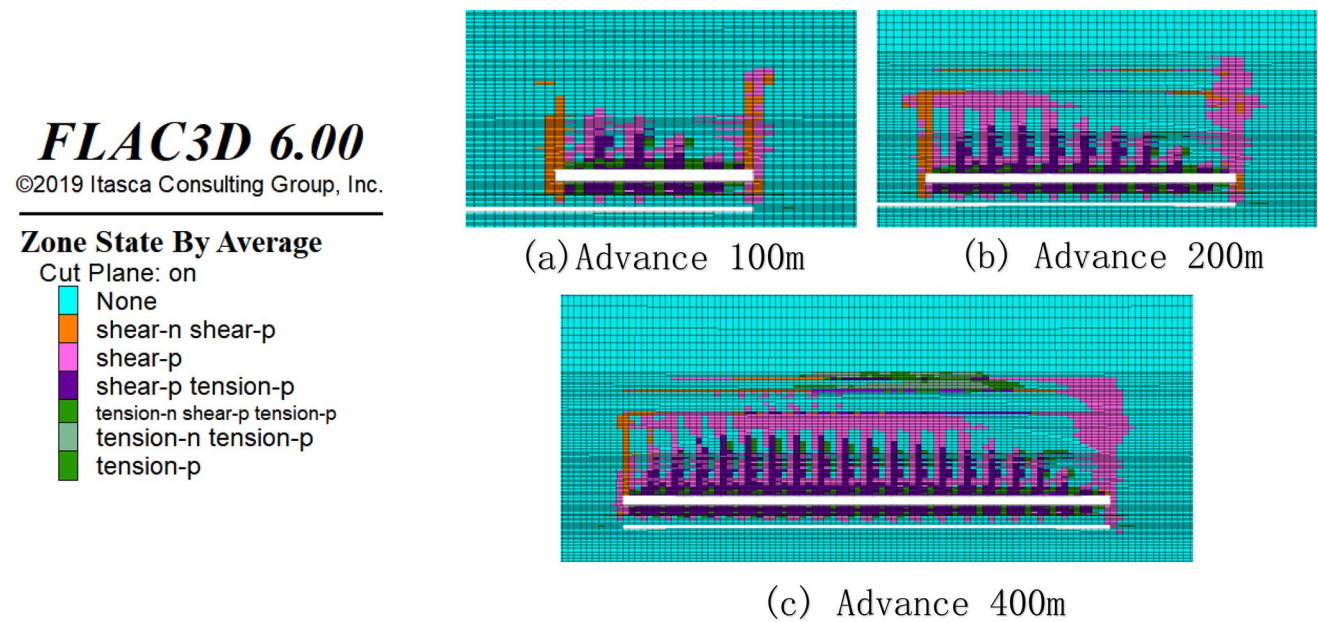
When  $M \leq h_1$ , the mining stress of the working face will shear damage the key layer, and the aquiclude after grouting will be transformed into a water storage layer again. Although it still has some blocking effect on the transmission of mining stress to the deep, it loses the ability to block water flow. When  $M > h_1$ , the key layer is less directly affected by the shear failure of mining stress and can block water flow.

- (2) Affected by the water lifting stress of deep aquifers

According to the mechanical analysis of water barrier by scholars, the following three conditions should be met to prevent tensile failure of key layers: the compressive strength ( $R_c$ ) of the key layer should be enhanced after grouting, the tensile strength ( $\sigma_3$ ) of the key layer should be greater than that of the deep aquifers, and the shear strength  $\sigma_1 \tan \varphi_k + c_k$  of the key layer should be greater than that of deep aquifers. The specific formula derivation process has been given by Lu et al. (2020).

- (3) Fault activation

Faults have the effect of cutting and destroying the integrity of rock layers and damaging the mechanical strength of the key layer. It is easy to fracture along the fault plane under mining stress, and when that happens,



**Fig. 8** Distribution of plastic zone in working face

the structural stability is lost. Meanwhile, due to the influence of mining, damage to the floor aquiclude will be further increased in the stress concentration area of the fault fracture zone. According to the MS scatter event analysis method, when the MS events in the fault fracture zone presents a vertical ‘point-line’ arrangement, it indicates that the fault is activated.

#### (4) Grouting reinforcement quality

The L8 limestone is a strong water-rich aquifer before grouting, so it is very important to ensure the grouting quality, which is the basis for transforming the strata to a key structurally stable water-control layer. According to engineering experience in the Jiaozuo mining area, the quality of grouting reinforcement is evaluated according to the ratio of the total water amount of the drilling holes and the total grout amount. Specifically, a flow of 60 m<sup>3</sup>/h should be grouted with at least 100 t of slurry.

### Influence Factors of the Floor Damage Infiltration Water Control Key Layer

#### (1) Effective water resistance layer thickness

The key floor infiltration water-control layer is mainly composed of mudstone, sandy mudstone, and other argillaceous soft rocks that prevents upward seepage of water

from the confined aquifer below. To be effective, it has to be sufficiently thick to be able to block the confined water.

The effective thickness of the key layer is directly related to the confined water pressure of the deep aquifer. According to the water bursting coefficient method, the thickness of the effective water-resisting layer,  $M = \frac{P}{T_s}$ , where  $P$  is the confined water pressure of deep aquifer, and  $T_s$  is the water inrush coefficient. Different coefficients are selected according to the working face conditions: 0.1 is used in normal sections and 0.06 is used in faulted areas. If the thickness of the key layer is less than the thickness of the effective water-resisting layer, it is judged to be unable to resist the lifting of the deep confined water by itself.

#### (2) Rock permeability

The grouting reinforcement is mainly aimed at the L8 aquifer; the grouting range in the rock mass below the aquifer is relatively limited. The initial fissures in this ungrouted rock mass damage its integrity. In addition, the natural cracks in the rock mass will continue to expand under the influence of the deep confined water and mining stress, even though the rock mass is partially screened from the latter by the upper stabilized layer.

In general, the resistivity of the same rock formation is generally stable. Low-resistance areas are typically fractured and water-rich, while high resistance areas are relatively dry. This allows TEM technology to be used to detect the degree of fracturing and rock mass permeability. According to experience in the Jiaozuo mining area, areas with an apparent

resistivity less than 10  $\Omega\cdot\text{m}$  have a relatively low resistance, and areas with an apparent resistivity greater than 100  $\Omega\cdot\text{m}$  are relatively high resistance.

### (3) Fault influence

The influence of fault on the key layer is mainly to destroy the integrity of rock mass and form water channel. The fracture of rock mass near the fault zone is developed, the permeability is enhanced, and it is more likely to fill water along the fault plane under the drive of deep confined water, resulting in water control failure. If the fault is activated under the influence of mining stress, the water channel will further expand, which will destroy the structural stability and water resistance of the key layer, resulting in a lack of infiltration water control. The water-richness and fault activation were respectively determined by the TEM and MS methods.

## Factors Influencing Weighting and Evaluation of 'Dual Key Layer' Water Control Capability

### Weight and Quantification of Factors Influencing the 'Dual Key Layer' Based on the AHP Method

#### Methodology

The analytic hierarchy process (AHP) decomposes the decision-related elements into multiple levels (such as objectives level, criteria level, and schemes level), constructs a judgment matrix, and calculates the comprehensive weight of each scheme on the objectives. The method has been widely used in groundwater spring potential zonation, evaluation of water inrush hazards and other mining and hydrogeology fields (Fan et al. 2023; Heydari et al. 2023; Prem et al. 2023; Xiao et al. 2023a, b).

Application of AHP usually is divided into three main steps. The first step is to construct a hierarchical model and define the evaluation indexes of different inputs. The second step is to construct a judgment matrix and assign weights according to field experience, previous studies, and expert opinions. As shown in Table 4, usually the Saaty's 1–9 scale method is used for allocation (Saaty 1994). The third step is the single hierarchical ranking and its consistency test, which determines the weight of the index (Waikar and Nilawar 2014), and its judgment formula is as follows:

$$CR = \frac{CI}{RI} \quad (6)$$

$$CI = \frac{\text{Maximum Principal Eigenvalue} - \text{Number of Factors}}{\text{Number of Factor} - 1} \quad (7)$$

where:  $CR$  is consistency ratio;  $CI$  is the consistency indicator, and the greater the value, the greater the degree of matrix deviation from consistency;  $RI$  is the random consistency index (see Table 5). When  $CR < 0.1$ , it is considered that the judgment moment matrix has good uniformity; otherwise, the judgment matrix needs to be adjusted until the consistency check is met.

#### The AHP Model Construction

The water control capability of the 'dual key layer' is the target layer of the model. It is divided into two criterion layers: the key structurally stable floor water control layer and the key infiltration-water damage-control floor layer. The sub-criterion layer includes four factors that influence the key structurally stable floor water control layer: spatial relationship (SR), stress effect (SE), fault activation (FA), and grouting reinforcement quality (GRQ); and three factors that influence the key infiltration-water damage-control floor layer: the effective water resistance layer thickness (LT), permeability (P), and fault influence (FI). The scheme layer is defined by two kinds of results: effective and ineffective 'dual key layers'. The weight of each factor under these two results is obtained by matrix calculation.

#### AHP Judgment Matrix and Results

Based on experience in the Jiaozuo mining area, the judgment matrix and the weight of each factor were established by using a scoring method and the above indicators, as shown in Tables 6, 7 and 8. According to the weight calculation results of the AHP in Table 6, among the influencing factors of key structurally stable floor water control layer, the weight of SR is 10.4%, the weight of SE is 5.5%, the weight of FA is 60.7%, and the weight of GRQ is 23.4%. The maximum weight of an indicator is FA (60.7), and the minimum weight is SE (5.5). The maximum principal eigenvalue is 4.2. According to Table 5, the  $RI$  value is

**Table 4** Saaty's 1–9 relative importance scale (Saaty 1994)

9/1	1/7	5/1	3/1	1	3	5	7	9
Extreme less importance	Very strong	Strong	Moderate	Equally equal	Moderate more important	Strong	Very strong	Extreme



**Table 5** RI value corresponds to the order n of matrix

n	3	4	5	6	7	8	9	10
RI	0.58	0.90	1.12	1.24	1.32	1.41	1.45	1.49

**Table 6** Judgment matrix and calculation results of floor structure stability water control key layer

	SR	SE	FA	GRQ	Weigh (%)
SR	1	3	0.143	0.333	10.4
SE	0.333	1	0.167	0.2	5.5
FA	7	6	1	4	60.7
GRQ	3	5	0.25	1	23.5

0.9. Therefore,  $CR = CI/RI = 0.09 \leq 0.1$ , which passes the consistency check.

As shown in Table 7, among the factors influencing the key infiltration-water damage-control floor layer, the weight of LT is 18.8%, the weight of P is 8.1%, and the weight of FI is 73.1%. The maximum value of index weight is FI (73.1) and the minimum value is P (8.1). The maximum principal eigenvalue is 3.1. According to Table 5, the RI value is 0.5,  $CR = CI/RI = 0.06 \leq 0.1$ , which passes the consistency check.

Table 8 shows the weight calculation results of the AHP scheme layer and analyzes the weight of each index (influencing factor) under different schemes. In the effective scheme of the ‘dual key layer’, grouting reinforcement quality (GRQ) has the greatest weight, while in the ineffective scheme with double key layers, fault activation (FA) and fault impact (FI) have the greatest weight.

### MS Characteristics of the Two Floor Zones in the Fault-influenced Region

According to the AHP method, fault activation and fault influencing factors play a crucial role in the failure of the ‘dual key layer’ water control. The characteristics of the ‘dual key layer’ under the influence of faulting were analyzed through MS event analysis.

#### Distribution Characteristics

171 MS events were detected in the two fault regions. The number of MS events occurring at different depths of the floor were counted; the relationship diagram is shown in Fig. 9. It can be seen that the number of MS events decreased gradually with depth. Of the 171 MS events, 84 occurred in the floor failure zone, accounting for 49% of the total. There were 65 MS events below the floor failure

**Table 7** Judgment matrix and calculation results of floor damage infiltration water control key layer

	LT	P	FI	Weigh (%)
LT	1	3	0.2	18.9
P	0.333	1	0.143	8.1
FI	5	7	1	73.0

**Table 8** Judgment matrix and calculation results of scheme layer

Influence Factor	Effective	Ineffective
SR	0.8	0.2
SE	0.8	0.2
FA	0.1	0.9
GRQ	0.9	0.1
LT	0.8	0.2
P	0.8	0.3
FI	0.1	0.9

zone to the L8 limestone bottom interface, accounting for 38%, and 22 MS events below the L8 limestone, accounting for 12%.

The numerical characteristics of the floor MS events are closely related to the floor failure depth; the number of MS events in the floor failure zone was the largest due to the direct influence of rock breaking stress after mining. Compared with the normal region, the number of MS events between the L8 limestone bottom interface and the floor failure zone significantly increased; the proportion in each region increased by 32%, indicating that the floor failure depth increased observably under the influence of faults. The number of MS events below the L8 limestone showed a steep decline; the number decreased by 85%, which shows that the grouting-reinforced L8 limestone provided structural stability, blocking energy transfer to below.

In the F15-15 fault zone, a MS event occurs every 15 m at depths of 61–120 m, down to the L2 limestone, indicating that a penetrating low-energy rock mechanically damaged zone had formed and that a water conduction channel may have formed under the combined influence of the fault and deep confined water lift.



## Morphological Characteristics of MS Events in Faulted Regions

### (1) Characteristics of MS events in water-conductive fracture zones

As shown in Fig. 10, the floor MS events of 15,091 working face fault regions are generally divided into two vertical distribution layers. The first layer is in the range of the floor failure zone. As shown in Fig. 10a, b, the high-density area of floor MS events was concentrated in the tension failure zone of the roadways and the hanging side of the fault. In Fig. 10c, d, under the influence of the fault in the middle of the working face, the MS events distribution characteristics have the shape of an ‘inverted triangle’. Under the traction of the faults, some MS events extended to below the floor failure zone.

The second layer was between the floor failure zone and the L8 limestone bottom interface. The number of MS events in the second layer is 22% less than that in the first layer and the high-density cloud does not extend to this area. As shown in Fig. 10, the MS events at this layer are generally parallel to the L8 limestone and gather at the top interface or inside the L8 limestone. It can be concluded that this form is mainly influenced by the mechanical barrier key layer of the L8 limestone.

### (2) Characteristics of MS events in the mechanical strength damaged zone

According to the above analysis, the mechanical strength damaged zone of the 15,091 working face was mainly located between the L8 and L2 limestones, and the MS events were

mainly affected by the mining stress ‘filtered’ L8 limestone, the lifting stress of the L2 limestone confined water, and fault activation. As shown in Fig. 10, the MS events were discrete in this zone, and no density cloud formed. There are obvious differences in MS events between F15-14 fault zone and F15-15 fault zone:

It can be seen in Fig. 10c that there was only one high-energy MS event in the deep fault area of F15-14, which is located on the fault plane below the L2 limestone, and there were no other deep MS events. Therefore, it can be concluded that no water-connecting channel had formed along the fault plane.

As shown in Fig. 10d, a number of MS events occurred in the zone between the L2 limestone aquifer and the working face (orange dashed line in Fig. 10d), showing a ‘point-line’ arrangement, which indicates that fault activation occurred during the mining process and that a water connecting channel had formed.

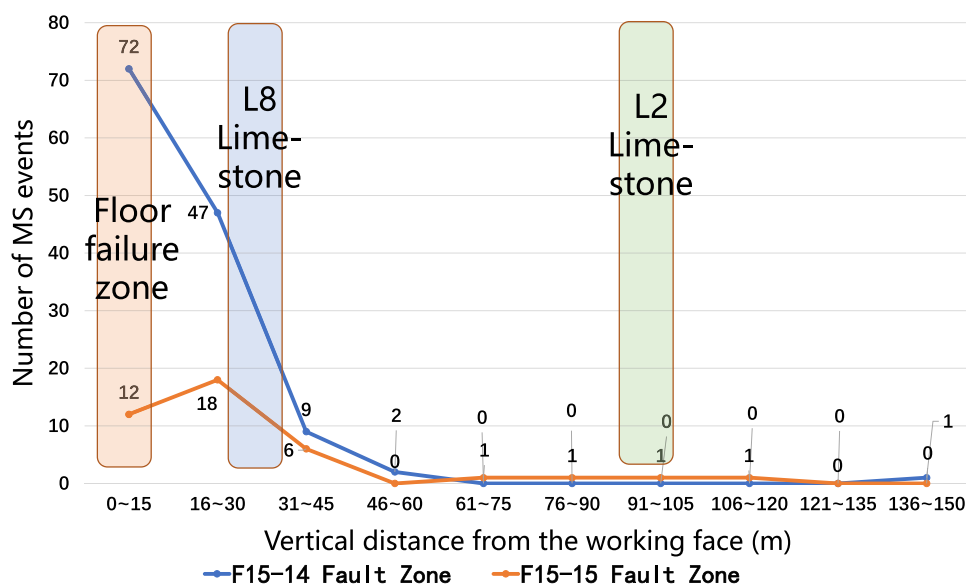
## Evaluation of 15,091 Working Face ‘Dual Key Layer’ Water Control Capability

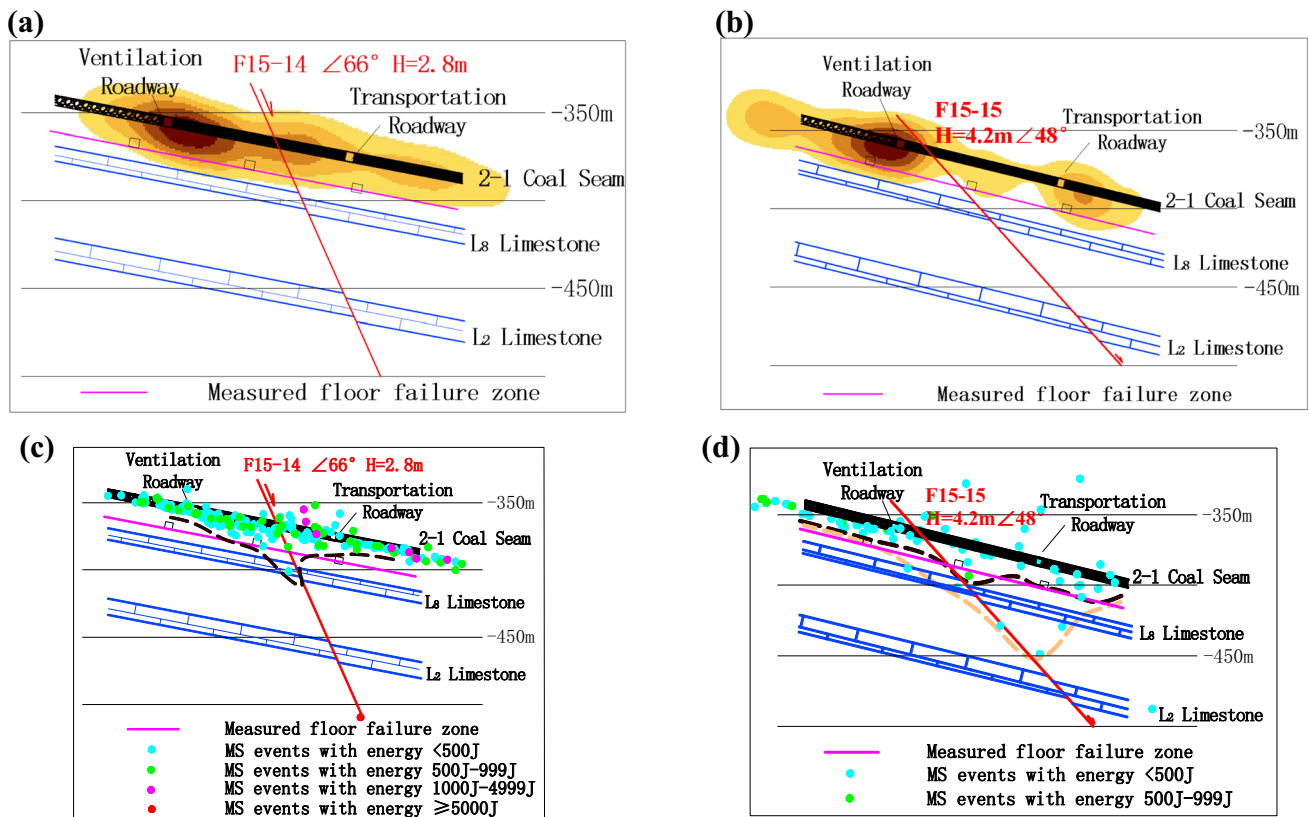
### Analysis of Influence Factors

#### (1) Spatial relationship

According to the previous analysis, the floor failure depth ( $h_f$ ) of the 15,091 working face floor was 15 m and the distance ( $M$ ) from the structure stability key layer (the reinforced L8 limestone) to the working face was 23 m,  $M > h_f$ , which indicates the key layer had the effect of blocking and water control.

**Fig. 9** Relationship diagram of MS events number and vertical distance in fault zone





**Fig. 10** 15,091 working face floor MS events profile of fault zone. **a** MS events density cloud map of F15-14 fault zone. **b** MS events density cloud map of F15-15 fault zone. **c** Scatter plot of MS events of F15-14 fault zone. **d** Scatter plot of MS events of F15-15 fault zone

## (2) Stress Influence on the structure stability key layer

According to the mine data, the internal friction angle ( $\varphi$ ) of the rock layer is  $40^\circ$ , the cohesion force ( $C$ ) is 16 MPa, and the average bulk density of the overlying rock layer ( $\gamma$ ) is  $2.4 \times 104 \text{ kN/m}^3$ . According to Table 3, the weighted average compressive strength ( $\bar{R}_c$ ) of the reinforced L8 limestone below the 15,091 working face was 26.6 MPa. The ratio of compressive strength ( $R_c$ ) and tensile strength ( $R_t$ ) of the key layer was obtained by the Mohr–Coulomb failure criterion:

$$\frac{R_c}{R_t} = \tan^2\left(45^\circ + \frac{\varphi}{2}\right) \quad (8)$$

The maximum allowable shear stress and tensile stress of key layer reinforced by grouting were 38.3 and 5.8 MPa, respectively. The calculated maximum shear stress and

tensile stress of the L2 limestone confined water of the 15,091 working face were 22.5 and 1.7 MPa, less than the allowable shear strength and tensile strength of the key layer. Therefore, the reinforced L8 limestone is able to resist the lifting stress of the L2 confined aquifer.

## (3) Grouting reinforcement quality

The 15,091 working face floor grouting reinforcement engineering was carried out before mining, and the reinforcement depth was 35 m below the L8 limestone. The total water amount of the drilling holes was  $808 \text{ m}^3/\text{h}$ , and the total grout amount was 3630 t. After conversion, 269.6 t of grout slurry was mixed with  $60 \text{ m}^3/\text{h}$  of water, which meets the engineering evaluation standard (a water flow of  $60 \text{ m}^3/\text{h}$  should be grouted with at least 100 t of slurry).

(4) Pressure resistance of the infiltration water control key layer

The key infiltration water control layer is the 43.5 m thick rock mass between the L8 limestone and L2 limestones. The upper 10 m of rock mass was reinforced by grouting, and the water inrush coefficient was calculated according to 0.1 MPa/m, while the unreinforced section was calculated according to 0.06 MPa/m. The comprehensive press resistance was  $35 \times 0.1 + 8.5 \times 0.06 = 4$  MPa, which exceeds the L2 limestone water pressure (3.8 MPa); therefore, the rock mass cracks does not tend to expand and connect under the normal influence of the L2 limestone water pressure.

(5) Permeability of the key infiltration water control layer

According to the floor TEM detection results after grouting of the 15,091 working face, two relatively low resistance area were detected in the internal slope angle of  $60^\circ$  from the transportation roadway (Fig. 11), and there was no relatively high resistance area in the working face. The X3-1 low resistance area is located between the L8 and L2 limestone strata, and intersects with the F15-15 fault, indicating that the L8 limestone contained little water after being grouted, but there were still water-filled cracks in the key infiltration water control layer in the F15-15 fault zone.

The second low resistance area, X3-2, was located in the L2 limestone, and there was no high or low resistance zone in the key infiltration water control layer nearby, indicating that the key infiltration water control layer has good permeability resistance in the F15-14 fault zone.

(6) Fault influence

According to the TEM detection, the F15-15 fault plane overlaps with the low-resistivity area, which indicates the water filled condition of the fault. In the F15-14 fault zone, there was no low resistance area above the L2 limestone, which indicates that the fault was relatively dry.

According to our analysis of MS characteristics in the faulted regions, there were a number of MS events showing a ‘point-line’ arrangement along the F15-15 fault plane, which indicates that the fault was activated and that a water conducting channel was likely to have formed.

The MS events of F15-14 fault were concentrated in the floor failure zone above the L8 limestone, and there no MS events extended to the deep area, which proves that its activation degree was limited and no water channel had formed.

### Evaluation and Verification of the Water Control Capability of the ‘Dual Key Layer’ in the 15,091 Working Face

(1) Comprehensive water control capability evaluation

A comprehensive evaluation of the water control ability of the 15,091 working face ‘dual key layer’ was carried out according to our analysis of the influence factors. The evaluation results are shown in Table 9.

In the key structurally stable floor water control layer, the SR, SE, and GRQ indexes were effective, accounting for 39.3% of the overall weight, while the FA index was

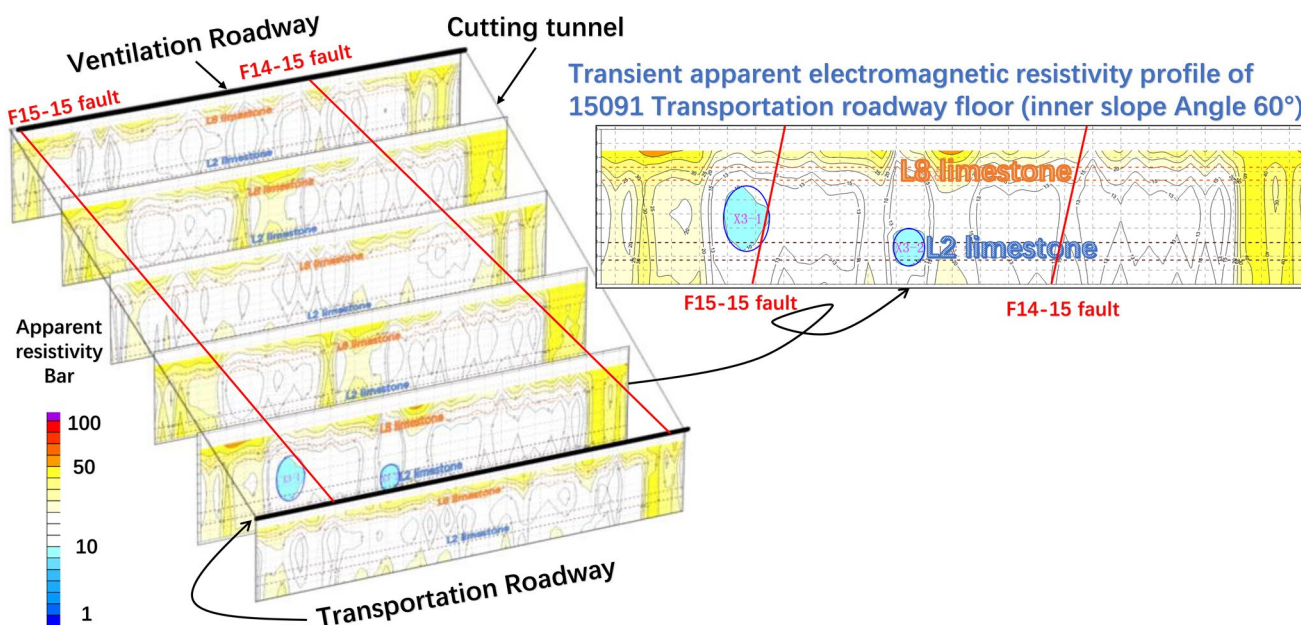


Fig. 11 15,091 working face floor transient electromagnetic detection results

**Table 9** Comprehensive evaluation of water control capability of the ‘dual key layer’ in 15,091 working face

Key layers	Influence factor	Weight (%)	Criteria for effective water control	Condition of working face	Single evaluation	Comprehensive evaluation
The floor structure stability water control key layer	Spatial relationship (SR)	10.4	The distance ( $M$ ) > 15.12 m( $h_1$ )	The distance ( $M$ ) is 23 m	Effective	The ‘dual key layer’ in most area of 15,091 working face is effective In $F_{15-15}$ fault zone is ineffective
	Stress effect (SE)	5.5	1. The compressive strength ( $R_c$ ) of the key layer is enhanced after grouting 2. The tensile strength is greater than 1.7 MPa 3. The shear strength is greater than 22.5 MPa	1. The compressive strength is enhanced by 40–159% 2. The maximum allowable tensile stress is 5.8 MPa 3. The maximum allowable shear strength is 38.3 MPa	Effective	
	Fault activation (FA)	60.7	Non-activation	$F_{15-15}$ fault is active	Ineffective	
	Grouting reinforcement quality (GRQ)	23.4	$\geq 100t$ grout slurry/ 60m <sup>3</sup> /h water amount	269.6t grout slurry/60m <sup>3</sup> /h water amount	Effective	
	Effective water resistance layer thickness (LT)	18.8	Resist 3.8 MPa water pressure	Resist 4 MPa water pressure	Effective	
The floor damage infiltration water control key layer	Permeability (P)	8.1	No transient electromagnetic high and low resistance area	One low resistance area intersects with $F_{15-15}$ fault zone	Ineffective	Ineffective
	Fault influence (FI)	73.1	1. No water filling 2. No activation	1. Part of $F_{15-15}$ fault plane is water-filling 2. $F_{15-15}$ fault is active	Ineffective	

ineffective, accounting for 60.7% of the overall weight, indicating that the key structurally stable floor water control layer can control water in most areas except for the F15-15 fault zone. In the area affected by the F15-15 fault, the key layer will fail to block the mining stress and confined water.

In the key floor damage infiltration water control layer, the index LT was effective, accounting for 18.8% of the overall weight, which indicates that the key layer can resist the water pressure of the deep confined water. The P and FI indexes were ineffective, accounting for 81.2% of the overall weight. The P and FI indexes coincide at the F15-15 fault zone, indicating that fault activation and fault water-filling are likely.

According to the results of the AHP judgment matrix and the analysis of influencing factors, in the non-faulted region of the 15,091 working face, the ‘dual key layer’ has the ability of water control, and the probability of floor water inrush is very small. In the F15-15 faulted area, the ‘dual key layer’ loses effectiveness, and the conditions for floor water inrush exist.

## (2) The verification

According to the mining situation of the 15,091 working face, when the working face advanced 404 m, passing the F15-15 fault zone, 24 m<sup>3</sup>/h of floor water surged from the transportation bottom roadway, and this flow remained stable until the end of the working face. The water inrush situation was consistent with the evaluation results.

## Summary and Conclusion

According to the changes of the mechanics and hydrogeological properties of the floor key rock strata after floor grouting, the coal seam floor was divided into two zones: a ‘water-conductive fracture zone’ and ‘mechanical strength damaged zone’. The composite water control model of a ‘key structurally stable floor water control layer’ and ‘floor damage infiltration water control key layer’ was established after grouting reinforcement of the uppermost subfloor aquifer.

MS technology was used to observe floor failure during mining. In the normal region, the floor failure was mainly affected by the mining stress of the working face and about 87% of the floor MS events occurred above the reinforced L8 limestone, showing an ‘inverted saddle-type’ stress distribution. In the faulted region, about 88% of the floor MS events occurred above the reinforced L8 limestone, but the number of MS events below the floor failure zone to the L8 limestone bottom interface increased by 32% compared with the normal region, indicating that the floor failure depth was increased by the faults. The MS events distribution had the shape of an ‘inverted triangle’ along the fault plane.

The elastic modulus of the floor rock mass before and after grouting was measured using the borehole ultrasonic method. The elastic modulus of the different rock mass after grouting reinforcement increased by 40–852%, respectively. Without floor grouting, the bottom failure depth of the experimental working face was 30.6 m, and the calculated bottom failure depth after reinforcement was 11.7 m. The maximum plastic failure depth calculated by FLAC3D numerical simulation method was about 17 m, and the MS monitoring result was 15 m. The floor failure depth measured by the direct current method was 15 m. The results show that the failure depth of the grouting reinforced floor was about 51% below than without grouting.

The AHP method was used to weight the seven factors that were believed to influence the floor water control ‘double key layer’: the SR, SE, FA, and GRQ index of the key structurally stable floor water control layer and the LT, P, and FI index of the key floor damage infiltration water control layer. The weight of SR was 10.4%, the weight of SE was 5.5%, the weight of FA was 60.7%, the weight of GRQ was 23.4% layer, the weight of LT was 18.8%, the weight of P was 8.1%, and the weight of FI was 73.1%. The results pass the consistency check. In the ineffective scheme with a dual key layer, fault activation (FA) and fault impact (FI) had the greatest weight.

The AHP and influencing factors methods were used to evaluate the dual key layer’ water control capability of the experimental working face. The results indicated that the floor ‘dual key layer’ in the non-faulted area controls the water and prevents a floor water inrush. In the faulted area, the floor ‘dual key layer’ is less effective and a floor water inrush is likely. The evaluation results were consistent with the actual water inrush situation of the working face.

**Acknowledgements** The authors are grateful to the Jiulishan coal mine for their partial funding, providing field testing sites, and related data. This work was supported by the National Natural Science Foundation of China (Fund 51934008).

**Data Availability** The data used to support the findings of this study are available from the corresponding author upon request.

## References

- Andrews K, Keim S (2021) Underground mine stream crossing assessment: a multi-disciplinary approach. *Int J Min Sci Technol* 31(1):59–65
- Fan R, Zhang H, Gao Y (2023) The global cooperation in asteroid mining based on AHP, entropy and TOPSIS. *Appl Math Comput* 437:127535
- He P, Liu CW, Wang C (2011) Correlation analysis of uniaxial compressive strength and elastic modulus of sedimentary rocks. *J Sichuan Univ (eng Sci Ed)* 43(04):7–12 (in Chinese)
- Heydari M, Osanloo M, Başçetin A (2023) Developing a new social impact assessment model for deep open-pit mines. *Resour Policy*. <https://doi.org/10.1016/j.resourpol.2023.103485>



- Hu Y, Li W, Wang QQ, Liu SL, Wang ZK, Zhen K (2019) Evolution of floor water inrush from a structural fractured zone with confined water. *Mine Water Environ* 38:252–260
- Huot F, Lellouch A, Given P, Bin L, Clapp RG, Tamas N, Nihei KT, Biondi BL (2022) Detection and characterization of microseismic events from fiber-optic DAS data using deep learning. *Seismol Res Lett* 93(5):2543–2553
- Li CY, Zuo JP, Huang XH, Wu GS, Li YB, Xing SK (2022) Water inrush modes through a thick aquifuge floor in a deep coal mine and appropriate control technology: a case study from Hebei, China. *Mine Water Environ* 41:954–969
- Liu C, Zhang PS, Ou YC, Yao DX, Tian YT (2022) Analytical stress analysis method of interbedded coal and rock floor over confined water: a study on mining failure depth. *J Appl Geophys*. <https://doi.org/10.1016/j.jappgeo.2022.104720>
- Lu HF, Meng XS, Zhang Y (2020) Mechanical analysis of water barrier performance of floor layered structure key stratum on coal face. *J China Univ Min Tech* 49(06):1057–1066 (in Chinese)
- Ma K, Yuan FZ, Wang HB, Zhang ZH, Sun XY, Peng YL, Wang HY (2021) Fracture mechanism of roof key strata in Dongjiahe coal mine using microseismic moment tensor. *Geomat Nat Hazards Risk* 12(1):1467–1487
- Miao W, Zhao L, Liu SQ, Jiang WH, Zhang EM, Li JK (2022) Roof failure mechanism of thin bedrock working faces under loading and analysis based on microseismic monitoring technology. *Geofluids*. <https://doi.org/10.1155/2022/7566637>
- Michas G, Vallianatos F (2020) Scaling properties and anomalous diffusion of the Florina micro-seismic activity: fluid driven? *Geomech Energy Environ* 24:100155
- Mu WQ, Li LC, Zhang YS, Yu GF, Ren B (2023) Failure mechanism of grouted floor with confined aquifer based on mining-induced data. *Rock Mech Rock Eng* 56:2897–2922
- Prem R, Kumar PP, Pandey V (2023) Groundwater spring potential zonation using AHP and fuzzy-AHP in eastern Himalayan region: Papum Pare district, Arunachal Pradesh, India. *Environ Sci Pollut Res*. <https://doi.org/10.1007/s11356-023-26769-w>
- Quiel SE, Naito CJ, Fallon CT (2019) A non-emulative moment connection for progressive collapse resistance in precast concrete building frames. *Eng Struct* 179:174–188
- Saaty TL (1994) How to make a decision: the analytic hierarchy process. *Interfaces* 24(6):19–43. <https://doi.org/10.1287/inte.24.6.19>
- Waikar ML, Nilawar AP (2014) Identification of ground water potential zone using remote sensing and GIS techniques. *Int J Adv Res Publ* 3(5):12163–12174. <https://doi.org/10.21474/ijar01/7116>
- Xiao L, Li F, Niu C, Dai G, Qiao Q, Lin C (2023a) Evaluation of water inrush hazard in coal seam roof based on the AHP-CRITIC composite weighted method. *Energies* 16:114. <https://doi.org/10.3390/en16010114>
- Xiao ZM, Gu ST, Zhang YX, Wang H (2023b) An effective control method of rock burst induced by shear instability of fault structure under complicated geological conditions. *Bull Eng Geol Environ* 82:105. <https://doi.org/10.1007/s10064-023-03119-1>
- Xu YC, Xie XF, Liu SQ (2017) Quantitative determination of mechanical property of “enhance-damage” for floor rock mass in grouting reinforcement working face. *J Min Safe Eng* 34(06):1186–1193 (in Chinese)
- Xu TF, Liang X, Xia Y, Jiang ZJ, Fabrizio G (2022) Performance evaluation of the Habanero enhanced geothermal system, Australia: optimization based on tracer and induced micro-seismicity data. *Renew Energy* 181:1197–1208
- Zhai M, Bai H (2023) Precise application of grouting technology in underground coal mining: water inrush risk of floor elimination. *Environ Sci Pollut Res* 30:24361–24376
- Zhai ML, Bai HB, Wu LY, Wu GM, Yan XZ, Ma D (2022) A reinforcement method of floor grouting in high-water pressure working face of coal mines: a case study in Luxi coal mine, North China. *Environ Earth Sci* 81:28
- Zuo JP, Wu GS, Du J, Lei B, Li YB (2022) Rock strata failure behavior of deep Ordovician limestone aquifer and multi-level control technology of water inrush based on microseismic monitoring and numerical methods. *Rock Mech Rock Eng* 55:4591–4614

Springer Nature or its licensor (e.g. a society or other partner) holds exclusive rights to this article under a publishing agreement with the author(s) or other rightsholder(s); author self-archiving of the accepted manuscript version of this article is solely governed by the terms of such publishing agreement and applicable law.